Journal of Power Sources 204 (2012) 257–264

Contents lists available at SciVerse ScienceDirect

Journal of Power Sources

journal homepage: www.elsevier.com/locate/jpowsour

Synergistic effects of ZnO compact layer and $TiCl_4$ post-treatment for dye-sensitized solar cells

Niu Huang[a], Yumin Liu[a], Tao Peng[a], Xiaohua Sun[a], Bobby Sebo[a], Qidong Tai[a], Hao Hu[a], Bolei Chen[a], Shi-shang Guo[a,b,*], Xingzhong Zhao[a,b,*]

[a] School of Physical Science and Technology, Wuhan University, Hubei 430072, People's Republic of China
[b] Key Laboratory of Artificial Micro/Nano-Structures of Ministry of Education, Wuhan University, Hubei 430072, People's Republic of China

ARTICLE INFO

Article history:
Received 25 October 2011
Received in revised form 8 December 2011
Accepted 11 December 2011
Available online 24 December 2011

Keywords:
Dye sensitized solar cells
Zinc oxide compact layer
Titanium tetrachloride post-treatment
Electrical transport
Charge recombination

ABSTRACT

The interaction between ZnO compact layer and $TiCl_4$ post-treatment on TiO_2 photoelectrode for dye sensitized solar cell (DSSC) is investigated. Photoelectrode combined the two modifications is designated as ZnO + 2l + $TiCl_4$. It is found that after the $TiCl_4$ treatment the ZnO compact layer transforms to a bi-functional layer, which suppresses back electrons transfer from FTO to electrolyte and reduces the FTO/TiO_2 interfacial resistance. In addition, the newly formed TiO_2 coating generated by $TiCl_4$ post-treatment contains abundant and well dispersed Zn element, which further facilitates electron transfer at TiO_2 layer. Meanwhile, the electron lifetime in ZnO + 2l + $TiCl_4$ is the longest. Consequently, the overall energy conversion efficiency of the cell with ZnO + 2l + $TiCl_4$ is significantly enhanced to 8.9%, which is 8.8% higher than that with pure $TiCl_4$ post-treatment and 17.7% higher than that without any treatment. These results are verified by material characterization and corresponding opto-electrical properties measurements. Experimental results demonstrate this facile method is a more promising alternative to the conventional interface and surface modification in high efficient DSSCs.

1. Introduction

Dye sensitized solar cells (DSSCs) have been considered as a low-cost alternative to conventional silicon-based photovoltaic devices. They have attracted wide attention in academic research and industrial applications since Grätzel et al. [1] reported their breakthrough discovery in 1991. Generally, the power generation in DSSCs is based on photoexcitation of dye molecules, which injects the photoelectrons into a TiO_2 film that leads the electrons toward the external circuit [2]. A mesoporous nanocrystalline structure (TiO_2 nanoparticles constituting film) is essential in order to adsorb sufficient dye molecules for photoelectrons generation and favorably soak hole-carrying electrolyte into photoelectrode. However, it presents two detrimental factors [3]: (i) inefficient electrical transport through the nanocrystalline network, and (ii) high charge recombination. Several studies have endeavored to modify the TiO_2 mesoporous photoelectrodes by adding compact layer at FTO/TiO_2 interface, forming shell or coating on TiO_2 mesoporous film surface, and by doping.

A majority of FTO/TiO_2 interface modification employ TiO_2 as the compact film [4–6], which decreases the back reaction sites on FTO, and yields corresponding improvement of the performance of DSSC. It has been reported that introducing large bandgap semiconducting oxide compact layer to form a potential barrier between FTO substrate and TiO_2 mesoporous layer is feasible for further decrease of the FTO/TiO_2 interfacial charge recombination. Nb_2O_5 [7,8] and ZnO [9] compact layers improve open-circuit photovoltage and fill factor, and keep fairly good short-circuit photocurrent density. A conventional surface modification method is the growing of an extra TiO_2 layer onto the surface of the nanoparticles comprising the TiO_2 mesoporous layer [6,10–13]. The working principle of this coating, as mostly reported [10,12,13], is to improve electron transport across the TiO_2 mesoporous layer by enhancing the connectivity among TiO_2 particles. More recently, metal ions have been employed to tailor the electric conductivity of the photoelectrodes. As reported, a compact Nb-doped TiO_2 thin film has been used to modify the FTO/TiO_2 interface of DSSCs, which suppressed the charge recombination from FTO to electrolyte and reduced the interfacial resistance of FTO/TiO_2; hence the charge collection efficiency was further enhanced [14,15]. The electron mobility through TiO_2 mesoporous layer has also been improved by incorporation of atomic impurities into TiO_2 nanoparticles, such as Al [16], Zn [17], Nb [18], and Ta [19]. However, to the best of our knowledge, introducing atomic impurities into the extra TiO_2 layer (as a doped coating on TiO_2 mesoporous layer) and the interaction between

* Corresponding authors at: Key Laboratory of Artificial Micro/Nano-Structures of Ministry of Education, Wuhan University, Hubei 430072, People's Republic of China. Tel.: +86 27 87642784; fax: +86 27 87642569.
E-mail addresses: xzzhao@whu.edu.cn (Z.-x. Zhao), gssyhx@whu.edu.cn (S.-s. Guo).

0378-7753/$ – see front matter © 2011 Elsevier B.V. All rights reserved.
doi:10.1016/j.jpowsour.2011.12.027

FTO/TiO_2 interfacial modification and mesoporous layer surface modification have not been reported for enhancing the overall energy conversion efficiency of DSSC.

In this article, we combine interfacial modification (formed by adding ZnO compact layer to FTO/TiO_2 interface) with surface modification (by $TiCl_4$ post-treatment) on photoelectrode. The reaction between these two modifications is expected because of the instability of basic ZnO in acidic $TiCl_4$ solution. For comparison, photoelectrodes with the combined two modifications, photoelectrodes with single treatment and untreated photoelectrodes are measured by material characterization, current–voltage (*I–V*), dark current, electrochemical impedance spectra (EIS) and Open-circuit voltage decay (OCVD). It is found that, the formed coating on TiO_2 mesoporous layer by $TiCl_4$ post-treatment is not pure TiO_2 but contain abundant and well dispersed Zn element. Meanwhile, the functions of the two modifications will be changed by combining them together. Hence, the combined effect enhances the overall energy conversion efficiency of DSSCs.

2. Experimental details

2.1. Materials

TiO_2 powders (P25, 20–30 nm, Degussa AG, Germany), ethylene glycol (EG), citric acid (CA), Zinc acetate, ethanolamine (EA), ethylene glycol monomethyl ether, ethanol, HCl, $TiCl_4$ and propylene carbonate (PC) were obtained from Sinopharm Chemical Reagent Corporation (China). Lithium iodide (LiI, 99%), 4-tert-butylpyridine (TBP) and guanidine thiocyanate (GNCS) were purchased from Acros. Iodine (I_2, 99.8%) was obtained from Beijing Yili chemicals (China). The Ru dye, cis-di(thiocyanato)-bis(2,2′-bipyridyl-4,4′-dicarboxylate) ruthenium(II) (N719), was purchased from Solaronix (Switzerland). All the reagents used were of analytical purity. Fluorine-doped SnO_2 conductive glass (FTO) with sheet resistance 10–15 $\Omega\,sq^{-1}$ was purchased from Asahi Glass (Japan).

2.2. Preparation of P25 paste and ZnO films on FTO substrates (FTO/ZnO substrates)

TiO_2 paste was prepared by ball-milling P25 powder with EG for 24 h and then ball-milling the mixture with CA for another 24 h at room temperature. The molar ratio of P25:EG:CA adopted the reported ratio [20] of 7:24:6.

ZnO films were prepared using zinc acetate sol as reported previously [21]. In short, EA was added into 30 ml ethylene glycol monomethyl ether under stirring at room temperature for 30 min, then 6 g zinc acetate was added with the molar ratio of EA/Zinc acetate being 1:1. For preparation of ZnO films, the zinc acetate sol was spread via spin-coating on clean FTO substrates with 2300 rpm for 20 s and then sintered at 500 °C for 1 h. The thickness of the ZnO films was around 190 nm as measured by SEM cross section.

2.3. Preparation of photoelectrodes prior to dye adsorption

Photoelectrodes without $TiCl_4$ post-treatment were prepared by doctor-blading P25 paste on FTO (labeled as 2l) and FTO/ZnO (labeled as ZnO + 2l) substrates, respectively, followed by sintering at 500 °C for 1 h. To P25 mesoporous films with similar thickness, the edges of the conducting glass were covered with two layers of adhesive tapes. The thicknesses of these films were around 14.7 μm, as measured with a TalyForm S4C-3D profilometer (UK).

Photoelectrodes 2l and ZnO + 2l were post-treated by immersing them in 50 mM $TiCl_4$ aqueous solution and kept at 70 °C for 30 min, followed by rinsing with deionized (DI) water and annealed at 500 °C in air for 30 min. The $TiCl_4$ post-treated photoelectrodes 2l and ZnO + 2l, were then labeled 2l + $TiCl_4$ and ZnO + 2l + $TiCl_4$, respectively.

2.4. Photoelectrodes sensitized and device fabrication

The mesoporous electrodes were preheated at 120 °C for 30 min and then immediately immersed in 0.5 mM N-719/ethanol solution for 24 h at room temperature to allow complete dye adsorption. Afterwards, the electrodes were washed with ethanol to remove accumulated dye molecules. A sandwich-type DSSC configuration was fabricated by clipping the N719 dye-loaded P25 photoelectrode with platinum (Pt) counter electrode and introducing electrolyte between the electrodes, the Pt electrode prepared by sputtering method [22]. The electrolyte was composed of 0.05 M LiI, 0.03 M I_2, 0.1 M 1-propy-3-methylimidazolium iodide, 0.1 M GNCS and 0.5 M 4-tert-butylpyridine in mixed solvent of acetonitrile and PC (volume ratio: 1/1).

2.5. Materials characterization of the photoelectrodes

The morphologies of ZnO, ZnO + 2l and ZnO + 2l + $TiCl_4$ were observed by scanning electron microscopy (SEM). X-ray photoelectron spectrum (XPS) was used to determine the chemical characteristics of powder scraped from ZnO + 2l and ZnO + 2l + $TiCl_4$, respectively. The binding energy was calibrated by locating the peak of C 1s for adsorbed hydrocarbons at 284.8 eV. Energy-dispersive X-ray spectroscopy (EDS, GENESIS 7000) was used to determine Zn element dispersion in ZnO + 2l + $TiCl_4$. By ultrasonic dispersing the powder scraped from ZnO + 2l + $TiCl_4$ in deionized water, the morphology of the particles was observed by transmission electron microscopy (TEM). Characteristics changes of the mesoporous films, after interface or surface modification, were surveyed by BET and UV–vis spectra of dye solution desorbing the photoelectrodes with 0.02 M aqueous NaOH.

2.6. Photoelectrical characteristic of DSSCs

The cells were tested by employing a solar light simulator (Oriel, 91192) as the light source and a computer-controlled electrochemical workstation (CHI660C, CH Instruments) as the data recorder. The intensity of the incident light was calibrated by a Si-1787 photodiode (spectral response range: 320–730 nm). The active DSSC area was controlled at 0.25 cm^2 by a mask. Photocurrent–voltage characteristics (*J–V* curves) were measured. Electrochemical impedance spectroscopy (EIS) measurements were performed under the open voltage bias at illumination. The frequency range was 0.01–1 MHz and the magnitude of modulation signal was 0.01 V. Open-circuit voltage decay (OCVD) characteristics were measured by turning off the illumination in a steady state [23] quickly, and recording the transient V_{oc} every 100 ms.

3. Results and discussion

3.1. Material characterization of photoelectrodes

3.1.1. Material characterization of ZnO compact layer, ZnO + 2l

Fig. 1 shows SEM images of ZnO compact layer and ZnO + 2l. Fig. 1(a) shows the surface morphology of ZnO layer on FTO substrate. As can be seen from Fig. 1(a), the ZnO layer is flat and compact. Fig. 1(b) shows the cross section SEM image of ZnO + 2l, in which we can clearly distinguish ZnO layer from mesoporous P25 layer. The concentration of Zn element in ZnO + 2l detected by EDS was around 2.2 at% (Zn/Ti ratio).

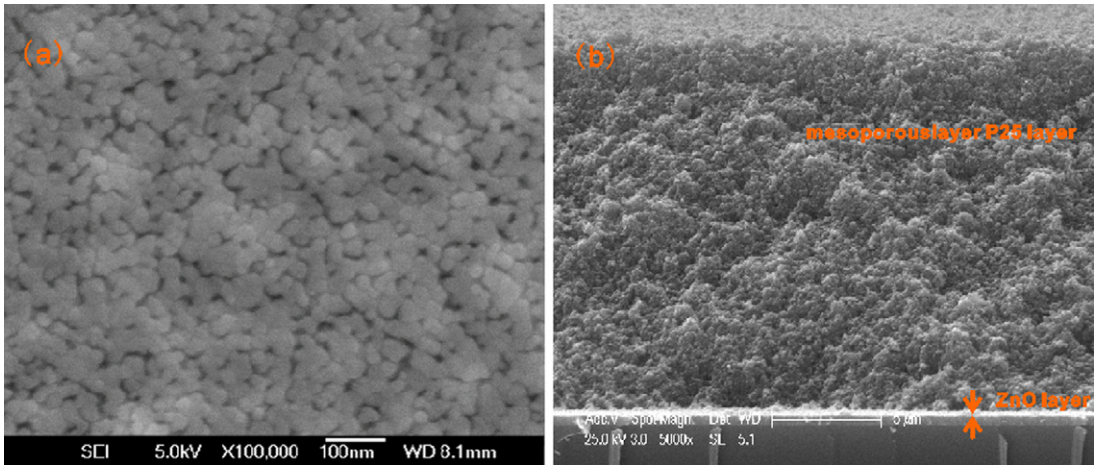

Fig. 1. (a) Surface SEM image of ZnO compact layer. (b) Cross section SEM image of ZnO + 2l.

3.1.2. *Material characterization of ZnO + 2l + $TiCl_4$*

Fig. 2(a) shows the SEM cross section image of ZnO + 2l + $TiCl_4$. As shown in Fig. 2(a), the ZnO layer could not be distinguished from the mesoporous layer. This indicates that the FTO/TiO_2 interface has been changed by $TiCl_4$ modification. Fig. 2(b) shows the cross section distribution of Zn element in ZnO + 2l + $TiCl_4$ acquired across the white line. No peaks are found in Fig. 2(b), which demonstrates that there is no gathering area of Zn element, which might mean Zn element is homogeneously distributed across the mesoporous P25 layer. Fig. 2(c) shows the XPS spectra of Zn $2p_{3/2}$ for powder scraped from ZnO + 2l and ZnO + 2l + $TiCl_4$. We can clearly identify the Zn $2p_{3/2}$ peak at 1021.4 eV for ZnO + 2l + $TiCl_4$, but cannot distinguish the Zn $2p_{3/2}$ peak for ZnO + 2l. The reason for this could be that the adhesion property between FTO underlayer and ZnO overlayer in ZnO + 2l remains relatively strong. Hence the powder scrapped from the photoelectrode ZnO + 2l comes mostly from mesoporous P25 layer which contains minute amount of ZnO. Fig. 2(d) shows the XPS spectra of Ti 2p. The Zn/Ti ratio of ZnO + 2l + $TiCl_4$ is 5.7 at% by comparing the peaks of Zn $2p_{3/2}$ with Ti $2p_{3/2}$.

Zn element exists in the mesoporous layer of ZnO + 2l + $TiCl_4$ with two probable formation processes: the first is as particles embedded in mesoporous TiO_2 layer, the second is as coating on the surface of TiO_2 nanoparticles, which constitute the mesoporous layer. Fig. 3 shows the TEM images of particles scraped

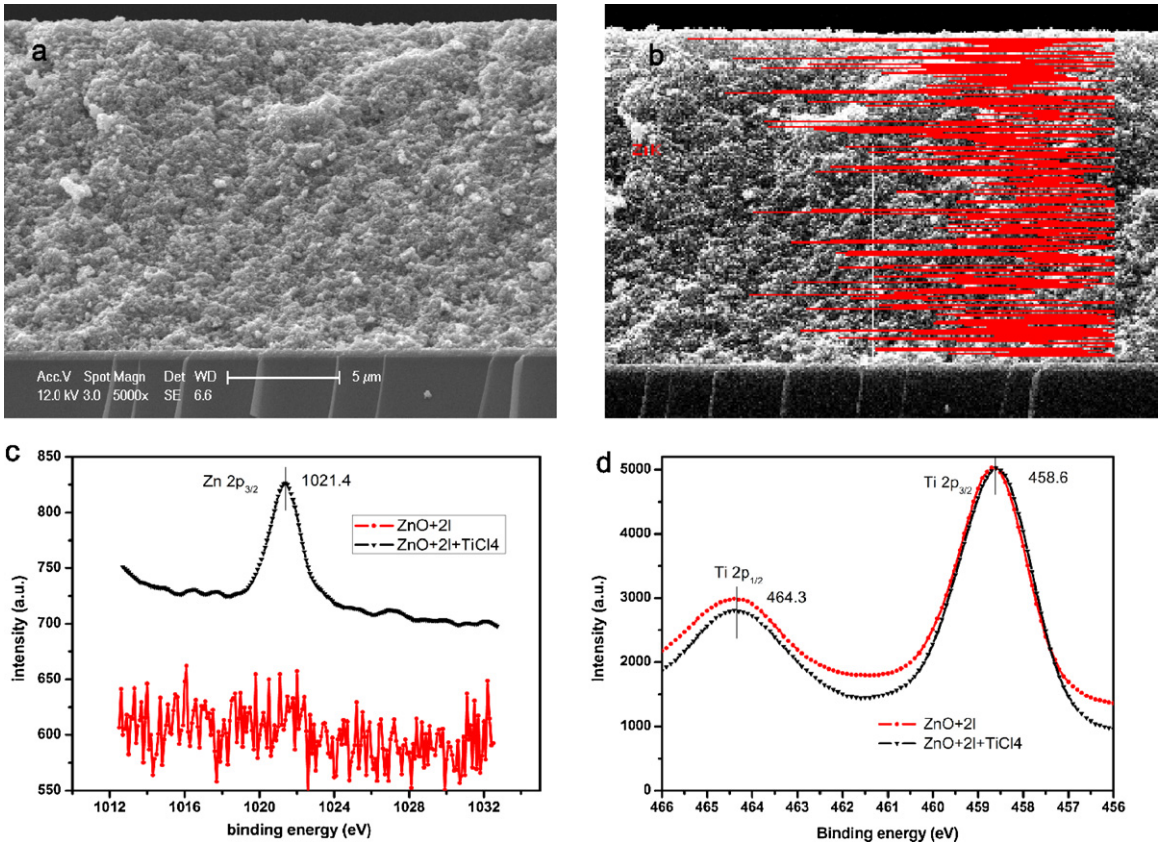

Fig. 2. (a) Cross section SEM images of ZnO + 2l + $TiCl_4$. XPS of powder scraping from ZnO + 2l and ZnO + 2l + $TiCl_4$, (b) Zn $2p_{3/2}$ of the two powder and (c) Ti 2p of the two powder. (d) EDS Zn element line profiles of ZnO + 2l + $TiCl_4$ acquired across ZnO + 2l + $TiCl_4$ noticed by the white line.

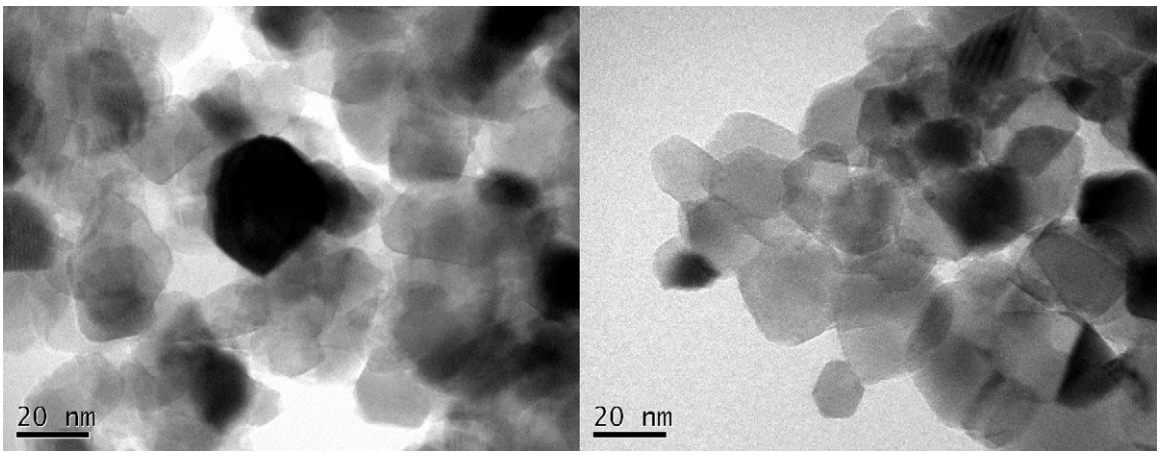

Fig. 3. TEM images of particles scraped from ZnO + 2l + $TiCl_4$.

from ZnO + 2l + $TiCl_4$, whose average size is around 25 nm in diameters. It is obvious that Zn/Ti ratio of ZnO + 2l + $TiCl_4$ is lower than the 2.2 at% Zn/Ti ratio of ZnO + 2l because part of ZnO in ZnO + 2l would be dissolved in the strong acidic $TiCl_4$ aqueous solution during $TiCl_4$ post-treatment. If Zn element exists as particles in ZnO + 2l + $TiCl_4$ with similar sizes as P25 nanoparticles, the Zn/Ti ratio of ZnO + 2l + $TiCl_4$ would be lower than 2.2 at% by XPS measurement, which is obviously contradictory to the result mentioned above (5.7 at%). Based on the above analysis, Zn element mostly exists as a coating on the mesoporous P25 layer in ZnO + 2l + $TiCl_4$. Owing to the fact that XPS survey provides surface analysis information, most of Zn elements would be probed while most part of Ti elements would be concealed, as a result the Zn/Ti ratio of ZnO + 2l + $TiCl_4$ by XPS is as high as 5.7 at% as reported above.

3.1.3. BET measurement of four different photoelectrodes

The film density, Brunauer–Emmett–Teller (BET) surface area, porosity and surface area of four types of photoelectrodes are shown in Table 1. It is found that, with the increase of film density of the electrodes by $TiCl_4$ post-treatment, the later three characteristic parameters of the electrodes all decrease [24]. However, these three parameters of ZnO + 2l + $TiCl_4$ are slightly higher than those of 2l + $TiCl_4$, which could be explained by the fact that the increase of mass of ZnO + 2l + $TiCl_4$ (3.2%) is much less than that of 2l + $TiCl_4$ (9.7%). The difference in mass increment could be explained from two aspects. On the one hand, some ZnO would dissolve in acidic $TiCl_4$ solution, which would lead the slight loss of mass of ZnO + 2l + $TiCl_4$. On the other hand, when Zn^{2+} is present in the aqueous solution, the specific adsorption of Zn^{2+} on TiO_2 nanoparticles could be expected [25,26], which would cause coating by Ti-hydroxide of $TiCl_4$ solution difficult. It is worth mentioning that Zn^{2+} adsorption onto TiO_2 nanoparticles and latter coverage by Ti-hydroxide may be a rational reason for abundant Zn element remaining as a coating formation in ZnO + 2l + $TiCl_4$.

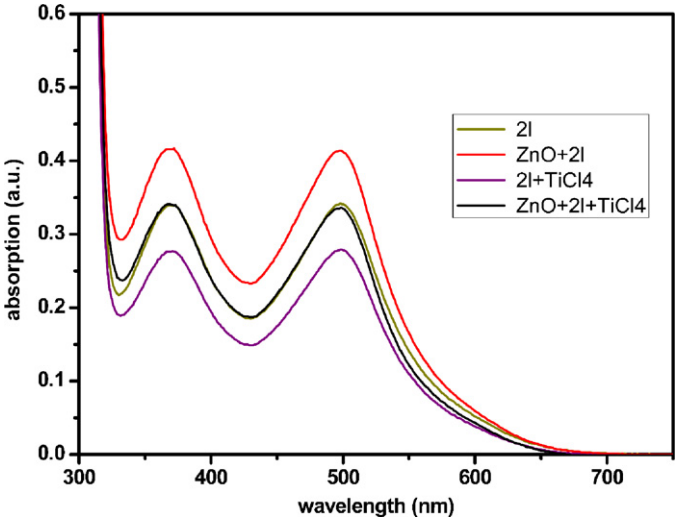

Fig. 4. UV–vis spectra of dye solution desorbed from 2l, ZnO + 2l, 2l + $TiCl_4$ and ZnO + 2l + $TiCl_4$, respectively.

3.1.4. UV-vis measurement for four different photoelectrodes

Fig. 4 shows UV–vis spectra of dye solution desorbed from photoelectrodes. As the surface area of photoelectrodes is decreased by $TiCl_4$ modification, as shown in Table 1, the amount of dye absorbed on 2l + $TiCl_4$ and ZnO + 2l + $TiCl_4$ is less than 2l and ZnO + 2l, respectively. While by adding ZnO compact layer, the absorption of ZnO + 2l and ZnO + 2l + $TiCl_4$ is much more than 2l and 2l + $TiCl_4$, respectively. This may be attributed to the higher basicity by containing the Zn element, which favors dye adsorption through carboxylic acid group of the N719 dye. As a result, the amount of dye adsorbed by ZnO + 2l + $TiCl_4$ equals to that absorbed by 2l.

Since ZnO + 2l + $TiCl_4$ photoanodes are processed $TiCl_4$ modification (the $TiCl_4$ aqueous solution contains high concentration of HCl), they would stable in acidic environment. It is found that

Table 1
Mass, BET, porosity and surface area characteristics of four different photoelectrodes.

Sample	Film density (g cm^{-3})	BET (m^2 g^{-1})	Porosity[a] (%)	Surface area[b] (m^2)	Mass increased by $TiCl_4$ mod.
2l	1.54	43.4	63.3	0.374	/
ZnO + 2l	1.57	43.1	62.6	0.379	/
2l + $TiCl_4$	1.69	33.8	59.8	0.319	9.70%
ZnO + 2l + $TiCl_4$	1.62	35.7	61.4	0.323	3.20%

[a] Porosity has been determined by comparing the film density to a density of 4.2 g cm^{-3} for bulk TiO_2.
[b] Electrode (internal) surface area was calculated by multiplication of the mass of a 4 cm^2, 14.7 μm TiO_2 film and BET.

Table 2
Photovoltaic performance parameters of DSSCs.

Sample	V_{oc} (mV)	J_{sc} (mA cm^{-2})	eff (%)	ff (%)
2l	758	14.04	7.36	65.7
ZnO + 2l	784	11.99	6.53	66.0
2l + $TiCl_4$	765	15.46	8.10	65.0
ZnO + 2l + $TiCl_4$	767	16.6	8.88	66.3

Table 3
Fitted parameters including R1 and R2 obtained by Zsimpwin software and electron lifetime calculated by f_{max} of Z2.

Sample	R1 (Ω)	R2 (Ω)	f_{max} of Z2 (Hz)	τ_e (s)
2l	4.18	14.61	3.742	0.0425
ZnO + 2l	6.62	15.4	6.643	0.0239
2l + $TiCl_4$	5.14	13.24	3.09	0.0516
ZnO + 2l + $TiCl_4$	3.57	13.16	3.09	0.0516

ZnO + 2l + $TiCl_4$ photoanodes are stable during the dye adsorption experiment, and the performances of ZnO + 2l + $TiCl_4$ DSSCs are stable in the whole measurement process.

3.2. The performance of DSSCs employing four different photoelectrodes

Fig. 5(a) shows the photocurrent density–voltage characteristics of DSSCs, while the photovoltaic performance parameters of the cells are listed in Table 2. The short-circuit photocurrent density (J_{sc}), open-circuit voltage (V_{oc}) and fill factor (ff) of 2l are 14.04 mA cm^{-2}, 758 mV and 65.7%, respectively, corresponding to an energy conversion efficiency (eff) of 7.36%. After a ZnO spin-coating film at the interface of FTO/TiO_2, ZnO + 2l gave an improvement of V_{oc} 26 mV, while J_{sc} decrease to 11.99 mA cm^{-2}, resulting in the eff decreased to 6.53%. After $TiCl_4$ post-treating of 2l, the J_{sc} of 2l + $TiCl_4$ was highly increased to 15.46 mA cm^{-2}, yielding an increase of eff to 8.1%. After combined two modification of photoelectrodes, ZnO + 2l + $TiCl_4$ gave an improvement of V_{oc} of 9 mV, ff increased to 66.3% and J_{sc} increased by 15.4% (from 14.04 to 16.6 mA cm^{-2}), finally resulting in the highest energy conversion efficiency of 8.9%, which was 17.1% higher than that of 2l and 8.8% higher than that of 2l + $TiCl_4$.

Fig. 5(b) shows the dark current–voltage characteristics of the DSSCs employing the 2l, ZnO + 2l, 2l + $TiCl_4$ and ZnO + 2l + $TiCl_4$ electrodes. The onset dark current occurs at low forward bias for 2l, whereas it shifts by a few hundred millivolts for ZnO + 2l, 2l + $TiCl_4$ and ZnO + 2l + $TiCl_4$. ZnO compact layer in ZnO + 2l can successfully reduce the back reaction sites on FTO substrate, and the dark current can be further suppressed by ZnO as the energy barrier because the conduction band edge of ZnO is more negative than TiO_2 [9]. $TiCl_4$ post-treatment of 2l (2l + $TiCl_4$) also can suppress the dark current by decreasing electron trap sites on TiO_2 surface [27], which is supported by the enhanced electron lifetime for recombination mentioned in Section 3.3.2. For the combined modification, the dark current of ZnO + 2l + $TiCl_4$ equals that of 2l + $TiCl_4$.

3.3. EIS and OCVD analyses

Electrochemical impedance spectroscopy (EIS) analysis is used to investigate the electron-transport and recombination in DSSCs. Fig. 6 shows EIS of DSSCs based on four different photoelectrodes. In the Nyquist plots of EIS spectra shown in Fig. 6(a), there are four sets of semicircles, each set comprising of a small one at high frequency and a large semicircle at low frequency. According to the EIS model reported in literature [8,28,29], the small semicircle which corresponds to the frequency range of 10^3–10^5 Hz (ω1) is ascribed to the charge transport at the FTO/TiO_2 and Pt counter electrode/electrolyte interfaces (Z1), the large semicircle in the low-frequency region is related to the electron transport within mesoporous layer and across TiO_2/electrolyte interface (Z2). The small semicircle is fitted to a charge-transfer resistance (R1) and a constant phase (Q1), and the large semicircle is fitted to a transport resistance (R2) and a constant phase (Q2) [28]. The fitted parameters including R1 and R2 obtained by Zsimpwin software are exhibited in Table 3. Since an identical Pt counter electrode was used for all the devices, the change at the interface of FTO/TiO_2 was considered mainly responsible for the difference of R1. As shown in Table 3, ZnO + 2l + $TiCl_4$ exhibits the lowest values for R1 and R2 resistances among the four types of DSSCs, which implies a more efficient charge-transfer process at the interface of FTO/TiO_2, at the dye-coated semiconductor/electrolyte interface and across the mesoporous layer. The Bode phase plots of EIS spectra, as shown in Fig. 6(b), display the frequency peaks of the charge transfer process at different interfaces of four different DSSCs. The characteristic low frequency peak (f_{max}) is located at 3.742 Hz for 2l, 6.643 Hz for ZnO + 2l, and 3.09 Hz for 2l + $TiCl_4$ and ZnO + 2l + $TiCl_4$, respectively. The electron lifetime for recombination (τ_e) of DSSC, as shown in Table 3, is determined by f_{max} values, where $\tau_e = \omega_{min}{}^{-1} = (2\pi f_{max})^{-1}$ [29]. An increased trend of τ_e is

$$\text{ZnO} + 2\text{l} < 2\text{l} < 2\text{l} + \text{TiCl}_4 = \text{ZnO} + 2\text{l} + \text{TiCl}_4.$$

Open-circuit voltage decay (OCVD) analysis is employed to measure recombination and electron lifetime in DSSCs, since the decay of photovoltage is mainly caused by the charge recombination [23]. Fig. 7 shows OCVD spectra of DSSCs based on the four different kinds of photoelectrodes. Fig. 7(a) shows the photovoltage transient spectra. The V_{oc} decays more slowly for ZnO + 2l + $TiCl_4$ and 2l + $TiCl_4$ samples, whereas it decays more quickly for ZnO + 2l compared with 2l. Fig. 7(b) shows the electron lifetime spectra of OCVD. The electron lifetime was calculated by the formula [23]

$$\tau = \frac{kT}{e}\left(\frac{dV}{dt}\right)^{-1} \quad (1)$$

As shown in Fig. 7(b), the electron life in ZnO + 2l + $TiCl_4$ is similar to that in 2l + $TiCl_4$, and is much higher than in 2l. The electron life in each of these three DSSCs is higher than in ZnO + 2l. It should be noted here that the variation trend of the electron lifetime measured by OCVD is the same as the EIS results. The lowest resistance for electron transport and the longest electron lifetime for recombination could favor the highest charge collection rate of photogenerated electrons [29], which led to the highest eff of ZnO + 2l + $TiCl_4$.

3.3.1. Electron transport and recombination at FTO/TiO_2 interface

R1 of 2l (4.18 Ω) is lower than that of 2l + $TiCl_4$ (5.14 Ω), and ZnO + 2l achieved the highest R1 resistance (6.62 Ω). This implies that the above two types of single modification do not facilitate the electron transfer across FTO/TiO_2 interface. The function of ZnO compact layer on DSSC was studied previously in detail [9]. In short, ZnO has a more negative conduction band edge than TiO_2 [3,11,24], which will suppress back electrons transfer from FTO to electrolytes. But this energy barrier would also block the electrons injection from the conductive band of TiO_2 to FTO. The blocking effect would lead to the increase of interfacial resistance of FTO/TiO_2 and the accumulation of electron in the conductive band of TiO_2. The high electron density in the conductive band of TiO_2 will aggravate the back reaction of electron in TiO_2 with I_3^- ions present in the electrolyte so that the electron lifetime for recombination (τ_e) of ZnO + 2l is lower than that of 2l.

In the case of ZnO + 2l + $TiCl_4$, R1 (3.57 Ω) is the lowest, which implies that the combined modification can reduce the interfacial resistance of FTO/TiO_2. In addition, the electron lifetime for

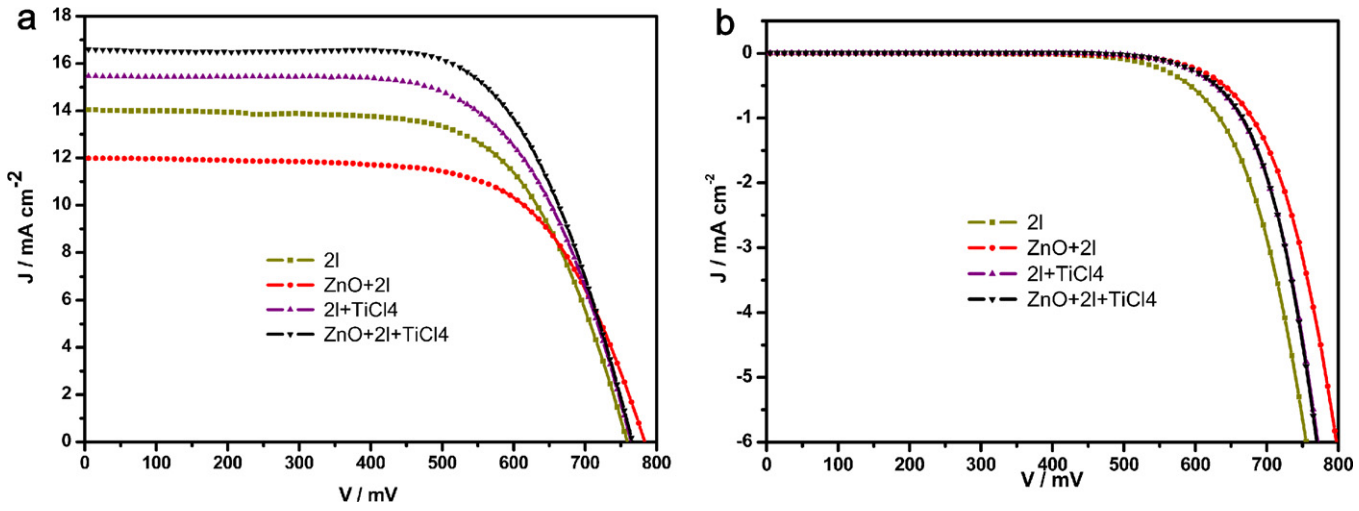

Fig. 5. Current density–voltage characteristics of DSSCs based on 2I, ZnO + 2I, 2I + $TiCl_4$ and ZnO + 2I + $TiCl_4$, respectively, (a) under AM 1.5 illumination 93.2 mW cm^{-2} and (b) under dark.

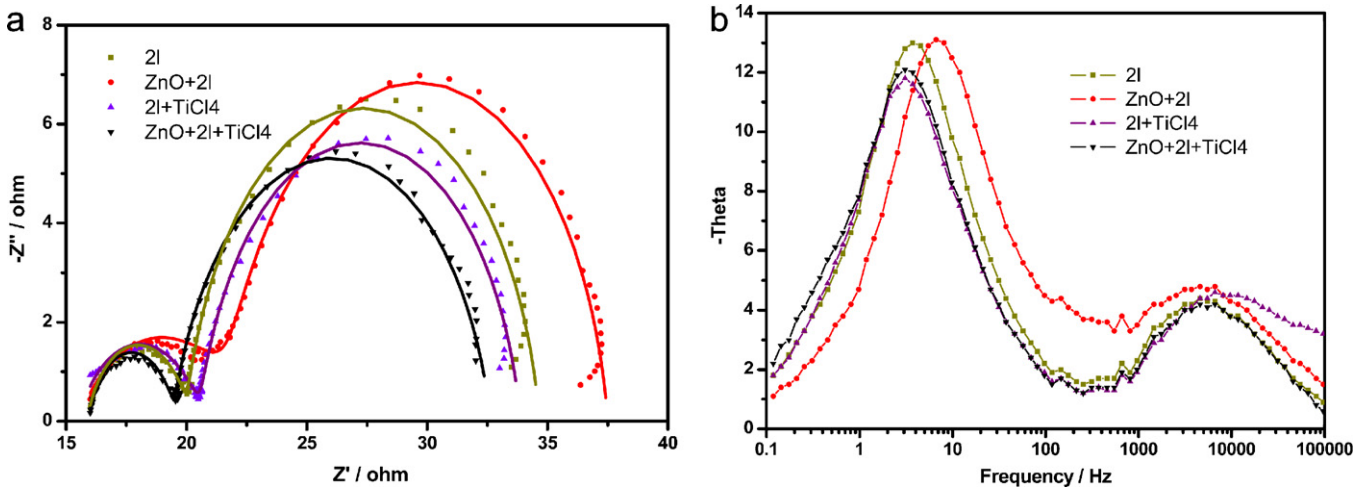

Fig. 6. EIS spectra of DSSCs based on 2I, ZnO + 2I, 2I + $TiCl_4$ and ZnO + 2I + $TiCl_4$, respectively, (a) Nyquist plots and (b) Bode phase plots. The symbols are experimental data, and the solid lines in (a) are fitted results.

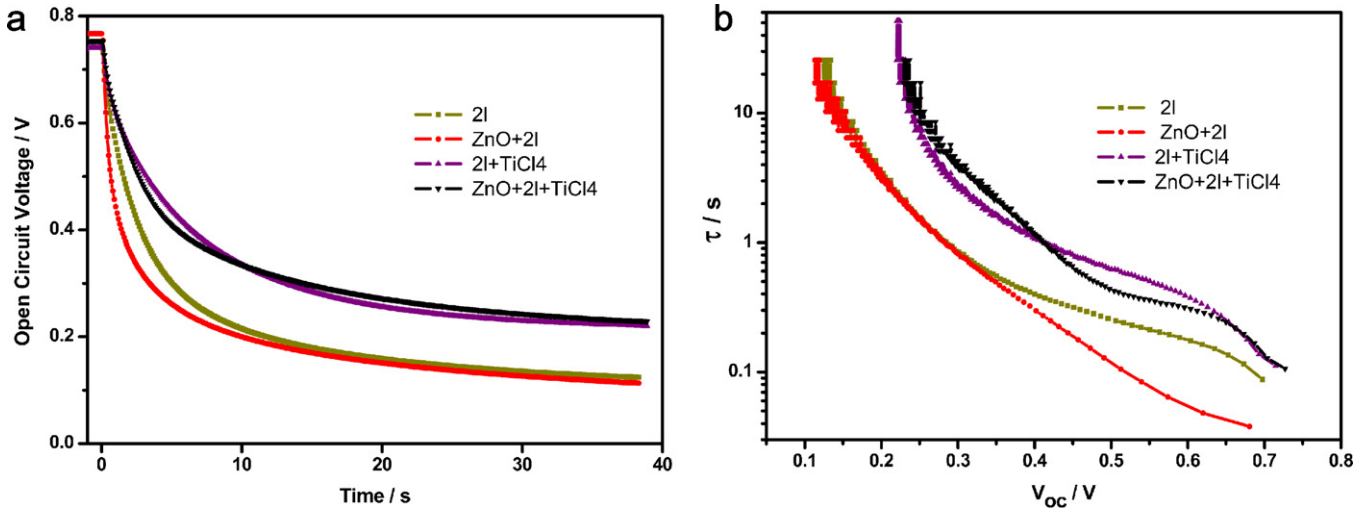

Fig. 7. (a) OVCD spectra of DSSCs based on 2I, ZnO + 2I, 2I + $TiCl_4$ and ZnO + 2I + $TiCl_4$, respectively. (b) The electron lifetime calculated from (a).

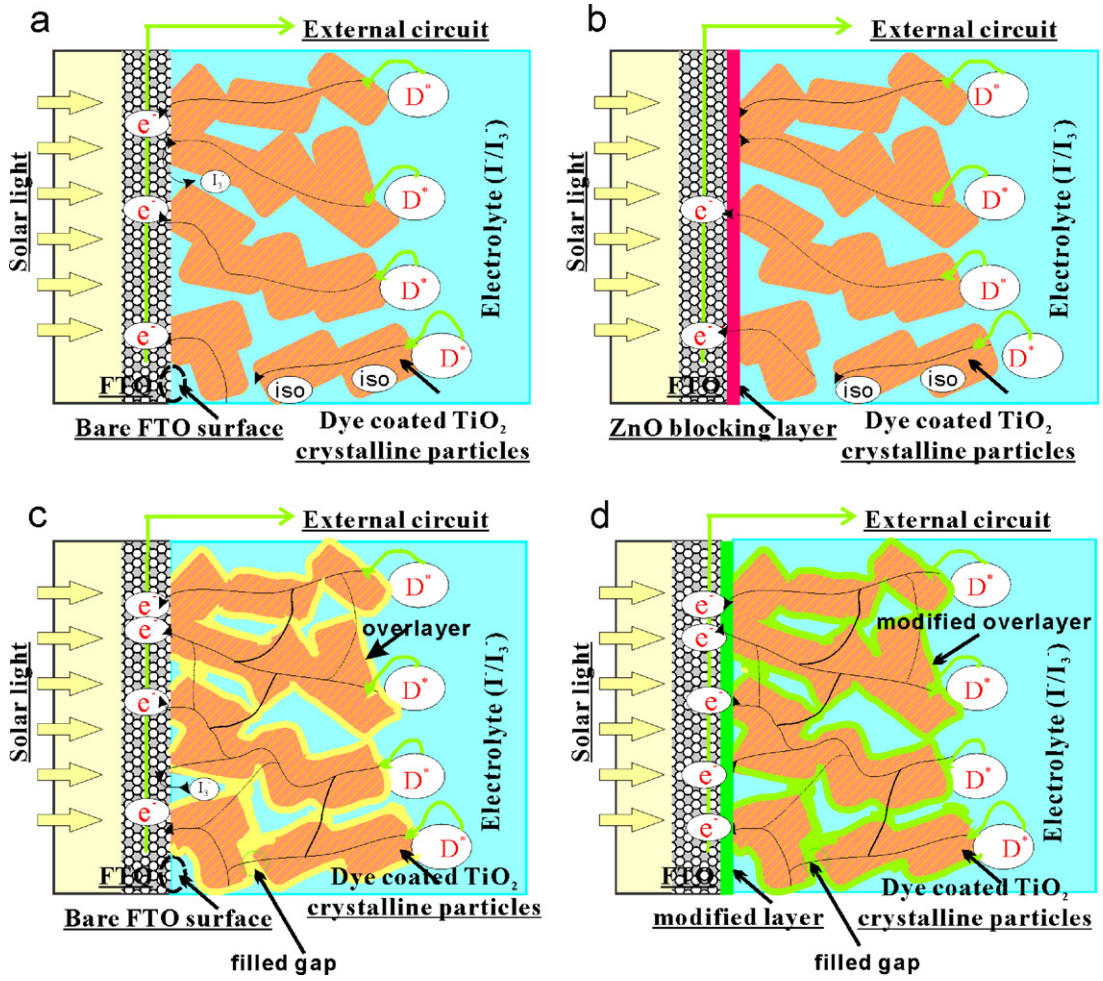

Fig. 8. Schematic diagrams of electron transport and recombination of photoelectrodes based on (a) 2I, (b) ZnO + 2I, (c) 2I + $TiCl_4$ and (d) ZnO + 2I + $TiCl_4$, respectively. (For interpretation of the references to color in text, the reader is referred to the web version of this article.)

recombination (τ_e) of ZnO + 2I + $TiCl_4$ increased when in comparison with 2I, while in the case of ZnO + 2I, it is decreased. This means the FTO/TiO_2 interface of ZnO + 2I + $TiCl_4$ would not lead to electron accumulation in the conductive band of TiO_2, but accelerate the transfer of electron from the conductive band of TiO_2 to FTO.

For the electron recombination at FTO/TiO_2 interface of ZnO + 2I + $TiCl_4$, the impurities in coating, as mentioned above in Sections 3.1.2 and 3.1.3, will facilitate electron back reaction with I_3^- ions. As a result, the electron recombination at mesoporous layer of ZnO + 2I + $TiCl_4$ will be higher than that of 2I + $TiCl_4$ with pure TiO_2 coating. Since the electron lifetime for recombination (τ_e) of ZnO + 2I + $TiCl_4$ equals that of 2I + $TiCl_4$, so as the dark current, the back reaction at FTO/TiO_2 interface of ZnO + 2I + $TiCl_4$ will be lower than that of 2I + $TiCl_4$ (The electron recombination with the triiodide occurs at two place: FTO/TiO_2 interface and mesoporous layer surface.). This means there would have an overlayer on FTO which can cover some exposed FTO surface to suppress back electrons transfer from FTO to electrolyte.

3.3.2. *Electron transport and recombination at mesoporous layer*

For 2I + $TiCl_4$, resistance of electron transport (R2) and back reaction of electron all decreased, the latter corresponding to the increase of electron lifetime for recombination, these changes illustrate the superiority and necessity of $TiCl_4$ modification [6].

In the case of ZnO + 2I + $TiCl_4$, the resistance of electron transport (R2) further decreased. After $TiCl_4$ post-treatment and later sintering, the coating on TiO_2 mesoporous layer surface contains some Zn element, as mentioned above in Sections 3.1.2 and 3.1.3, which would further facilitate the electron transport at TiO_2 mesoporous layer [17].

3.4. *Schematic views of electron transfer*

The schematic views of electron transfer with and without modification are shown in Fig. 8. The mesoporous nature of the nanocrystalline TiO_2 film would expose a portion of FTO surface to electrolyte, which leads to the direct back electrons transfer from FTO to electrolyte [30], as shown in Fig. 8(a) and (c). Furthermore, the poor connectivity of the nanocrystalline TiO_2 film would slow down the electron transport across the mesoporous layer, as shown in Fig. 8(a) and (b), and some TiO_2 particles are even isolated from electron pathways that are connected to the conducting substrates (i.e., particles marked with "*iso*" in Fig. 8) [12]. For single ZnO modification, as shown in Fig. 8(b), back electron transfer from FTO to electrolyte is effectively suppressed by covering the exposed FTO and functioning as energy barrier. However, the ZnO modification would also retard the electron injection from TiO_2 mesoporous layer to FTO (Red represents the blocking function.). For single $TiCl_4$ modification, as shown in Fig. 8(c), it widens electron pathways by cementing the TiO_2 nanoparticles together to favor electron transfer across mesoporous layer (Light yellow represents the cementing function of coating on mesoporous layer.). For the combined modification, as shown in Fig. 8(d), back electron transfer from FTO to electrolytes would be suppressed by covering the exposed FTO, at

the same time electron transfer across mesoporous layer is favored by the widened electron pathways. Moreover, electron transfer across mesoporous layer and injection from TiO_2 to FTO will be further favored by the synergistic effect (Green represents the facilitated electron transfer function of the synergistic effect between ZnO compact layer and $TiCl_4$ post-treatment.).

4. Conclusion

In summary, we have developed a methodology of photoelectrode modification by combining a basic ZnO compact layer with an acidic $TiCl_4$ post-treatment. After $TiCl_4$ post-treatment, the ZnO compact layer transformed to an bi-functional layer at FTO/TiO_2 interface, which suppressed back electrons transfer from FTO to electrolyte and reduced the interfacial resistance between mesoporous TiO_2 layer and FTO. In addition, after adding the basic ZnO overlayer on FTO, the newly formed coating on the surface of TiO_2 mesoporous layer was not pure TiO_2 but contained abundant Zn element, which further facilitated electron transfer and collection. As a result, the overall energy conversion efficiency of DSSC incorporating ZnO layer and $TiCl_4$ post-treatment was highly enhanced. These results strongly implies that the combined modification is a more attractive method to replace the conventional photoanodes' interface and surface modification for high efficiency DSSCs with high stable.

Acknowledgments

The authors would like to acknowledge the financial support of the National Basic Research Program of China (973 Program, 2011CB933300), and the partial financial support from the National Nature Science Foundation of China (Nos. 50125309 and 10804087).

References

[1] B. O'Regan, M. Grätzel, Nature 353 (1991) 737.
[2] P.T. Hsiao, Y.L. Tung, H.S. Teng, J. Phys. Chem. C 114 (2010) 6762.
[3] R. Jose, V. Thavasi, S. Ramakrishna, J. Am. Ceram. Soc. 92 (2) (2009) 289.
[4] H. Yu, S.Q. Zhang, H.J. Zhao, G. Will, P.R. Liu, Electrochim. Acta 54 (4) (2009) 1319.
[5] A.O.T. Patrocinio, L.G. Paterno, N.Y.M. Iha, J. Photochem. Photobiol. A 205 (1) (2009) 23.
[6] S. Ito, T.N. Murakami, P. Comte, P. Liska, C. Grätzel, M.K. Nazeeruddin, M. Grätzel, Thin Solid Films 516 (14) (2008) 4613.
[7] J.B. Xia, N. Masaki, K.J. Jiang, S. Yanagida, Chem. Commun. 2 (2007) 138.
[8] J.B. Xia, N. Masaki, K.J. Jiang, S. Yanagida, J. Phys. Chem. C 111 (22) (2007) 8092.
[9] Y.M. Liu, X.H. Sun, Q.D. Tai, H. Hu, B.L. Chen, N. Huang, B. Sebo, X.Z. Zhao, J. Power Sources 196 (2011) 475.
[10] L. Kavan, B. O'Regan, A. Kay, M. Grätzel, J. Electroanal. Chem. 346 (1993) 291.
[11] D. Menzies, R. Gervini, Y.B. Cheng, G.P. Simon, L. Spiccia, J. Aust. Ceram. Soc. 39 (2) (2003) 108.
[12] H. Yu, S.Q. Zhang, H.J. Zhao, B.F. Xue, P.R. Liu, G. Will, J. Phys. Chem. C 113 (2009) 16277.
[13] C.J. Barbe, F. Arendse, P. Comte, J. Am. Ceram. Soc. 80 (1997) 3157.
[14] S.W. Lee, J.H. Noh, H.S. Han, D.K. Yim, D.H. Kim, J.K. Lee, J.Y. Kim, H.S. Jung, K.S. Hong, J. Phys. Chem. C 113 (16) (2009) 6878.
[15] J.H. Noh, S. Lee, J.Y. Kim, J.K. Lee, H.S. Han, C.M. Cho, I.S. Cho, H.S. Jung, K.S. Hong, J. Phys. Chem. C 113 (3) (2009) 1083.
[16] K.H. Ko, Y.C. Lee, Y.J. Jung, J. Colloid Interface Sci. 283 (2005) 482.
[17] K.P. Wang, H.S. Teng, Phys. Chem. Chem. Phys. 11 (2009) 9489.
[18] X.J. Lu, X.L. Mou, J.J. Wu, D.W. Zhang, L.L. Zhang, F.Q. Huang, F.F. Xu, S.M. Huang, Adv. Funct. Mater. 20 (2010) 509.
[19] J. Liu, H.T. Yang, W.W. Tan, X.W. Zhou, Y. Lin, Electrochim. Acta 56 (2010) 396.
[20] U.O. Krašovec, M. Berginc, M. Hočevar, M. Topič, Sol. Energy Mater. Sol. Cells 93 (2009) 379.
[21] M.W. Zhu, J.H. Xia, R.J. Hong, H. Abu-Samra, H. Huang, T. Staedler, J. Gong, C. Sun, X. Jiang, J. Cryst. Growth 310 (2008) 816.
[22] C.H. Zhou, H. Hu, Y. Yang, B.L. Chen, J. Zhang, S.J. Wu, S. Xu, X.D. Xiong, H.W. Han, X.Z. Zhao, J. Appl. Phys. 104 (2008) 034910.
[23] J. Bisquert, A. Zaban, M. Greenshtein, I. Mora-Sero, J. Am. Chem. Soc. 126 (41) (2004) 13550.
[24] P.M. Sommeling, B.C. O'Regan, R.R. Haswell, H.J.P. Smit, N.J. Bakker, J.J.T. Smits, J.M. Kroon, J.A.M. van Roosmalen, J. Phys. Chem. B 110 (2006) 19191.
[25] S.S. Kim, J.H. Yum, Y.E. Sung, J. Photochem. Photobiol. A: Chem. 171 (2005) 269.
[26] A. Kay, M. Grätzel, Chem. Mater. 14 (2002) 2930.
[27] M.K. Nazeeruddin, A. Kay, I. Rodicio, R. Humphry-Baker, E. Müller, P. Liska, N. Vlachopoulos, M. Grätzel, J. Am. Chem. Soc. 115 (1993) 6382.
[28] Q. Wang, J.E. Moser, M. Grätzel, J. Phys. Chem. B 109 (31) (2005) 14945.
[29] Y.Z. Zheng, X. Tao, L.X. Wang, H. Xu, Q. Hou, W.L. Zhou, J.F. Chen, Chem. Mater. 22 (2010) 928.
[30] S. Ito, P. Liska, P. Comte, R. Charvet, P. Péchy, U. Bach, L. Schmidt-Mende, S.M. Zakeeruddin, A. Kay, M.K. Nazeeruddin, M. Grätzel, Chem. Commun. (2005) 4351.